Repeated Growth–Etching–Regrowth for Large-Area Defect-Free Single-Crystal Graphene by Chemical Vapor Deposition

Teng Ma,[†] Wencai Ren,[*,†] Zhibo Liu,[†] Le Huang,[‡] Lai-Peng Ma,[†] Xiuliang Ma,[†] Zhiyong Zhang,[‡] Lian-Mao Peng,[‡] and Hui-Ming Cheng[†]

[†]Shenyang National Laboratory for Materials Science, Institute of Metal Research, Chinese Academy of Sciences, 72 Wenhua Road, Shenyang 110016, People's Republic of China and [‡]Key Laboratory for the Physics and Chemistry of Nanodevices and Department of Electronics, Peking University, Beijing 100871, People's Republic of China

ABSTRACT Reducing nucleation density and healing structural defects are two challenges for fabricating large-area high-quality single-crystal graphene, which is essential for its electronic and optoelectronic applications. We have developed a method involving chemical vapor deposition (CVD) growth followed by repeated etching–regrowth, to solve both problems at once. Using this method, we can obtain single-crystal graphene domains with a size much larger than that allowed by the nucleation density in the initial growth and efficiently heal structural defects similar to graphitization but at a much lower temperature, both of which are impossible to realize by conventional CVD. Using this method with Pt as a growth substrate, we have grown ~3 mm defect-free single-crystal graphene domains with a carrier mobility up to 13 000 $cm^2 V^{-1} s^{-1}$ under ambient conditions.

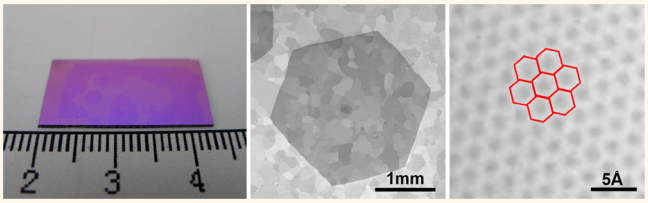

KEYWORDS: graphene · single crystal · large size · defect free · chemical vapor deposition

Graphene, an atomically thin two-dimensional carbon material, has been extensively demonstrated to be an ideal candidate for high-performance electronic and optoelectronic devices, such as high-frequency transistors, ultrafast photodetectors, and broadband optical modulators, because of its extraordinarily high carrier mobility, significant wavelength-independent absorption, high mechanical strength, highest recorded thermal conductivity, and good environmental stability.[1−4] Similar to the current Si-based electronics, the availability of wafer-size high-quality single-crystal graphene is fundamental for these applications because grain boundaries[5−11] and defects[12−16] significantly alter its properties.

Chemical vapor deposition (CVD) has shown great potential for fabricating large-area single-crystal graphene based on three general strategies. The first is to reduce the nucleation density of graphene domains to be as small as possible, providing enough space for graphene growth from one nucleus. Several approaches have been developed to reduce the nucleation density, such as electrochemical polishing[17,18] and high-temperature annealing of a Cu substrate,[17,19] using a Pt substrate with a high melting point and catalytic activity,[20] reducing the flow rate ratio of carbon precursor to hydrogen,[7,21] and tuning the reaction pressure,[22] introducing oxygen into reaction systems.[23−25] Using these approaches, centimeter-scale single-crystal graphene domains have been fabricated in the presence of oxygen.[23] The second strategy involves the catalytic and epitaxial growth of graphene on a single-crystal substrate. In this case, even though the graphene nucleation density is high, all the nuclei can grow and coalesce into single-crystal graphene without grain boundaries since they are perfectly aligned with each other on a single-crystal substrate with well-defined and anisotropic atomic arrangement. Wafer-scale single-crystal graphene has been fabricated on a silicon wafer by using a hydrogen-terminated germanium buffer layer

* Address correspondence to wcren@imr.ac.cn.

Received for review October 23, 2014 and accepted November 23, 2014.

Published online November 23, 2014
10.1021/nn506041t

based on this second strategy.[26] The third strategy is epitaxial growth from graphene domain seeds by two-step CVD, which involves a CVD growth followed by annealing or oxidation and a secondary growth.[27,28] It has been demonstrated that micrometer-sized graphene domain seeds can be amplified to millimeter-sized domains by this strategy;[27] however, many small additional layers were formed in the boundary areas between the graphene seeds and the epitaxially grown regions or on the surface of the graphene seeds.[27,28]

Although the nucleation density can be reduced by the first growth strategy, inevitably, some new nuclei appear during growth. Such random nucleation prohibits the further growth of single-crystal graphene domains, and theoretically it is impossible to obtain single-crystal graphene domains larger than the distance between the initial neighboring nuclei. The maximum size of the graphene domains by a two-step CVD method is also limited by the initial nucleation density. More importantly, many structural defects are present in the CVD-grown single-crystal graphene by all the above strategies. The existence of structural defects is actually a common problem for all graphene materials prepared by various methods including mechanical cleavage. They may appear during growth or processing and greatly deteriorate the performance.[12] For instance, the carrier mobility of CVD-grown single-crystal graphene reported so far is usually lower than 8000 $cm^2\ V^{-1}\ s^{-1}$ under ambient conditions based on back-gated field-effect transistors (FETs) on SiO_2/Si substrates (Table S1), and this is much lower than the theoretical value.[29,30] Knowing how to heal these defects is essential for graphene applications in electronics and optoelectronics and is still very challenging.

In our previous study, we found that the growth and etching of single-crystal graphene domains are reversible.[31] On the basis of this understanding, here, we develop a new method, CVD growth followed by repeated etching−regrowth (G−rE−RG), to fabricate large-area defect-free single-crystal graphene, where the methane flow rate does not remain the same but decreases with the number of growth cycles. Using this method, we can obtain single-crystal graphene domains with a size much larger than that allowed by the nucleation density in the initial growth and efficiently heal structural defects similar to what happens during graphitization but at a much lower temperature. Both of these are impossible to realize by conventional CVD (including the one-step and two-step CVD methods mentioned above). Using this method with Pt as the growth substrate, we have grown ~3 mm defect-free single-crystal graphene domains with a carrier mobility up to 13 000 $cm^2\ V^{-1}\ s^{-1}$ under ambient conditions. This is about double the best mobility reported so far for CVD-grown single-crystal graphene using similar measurement conditions.

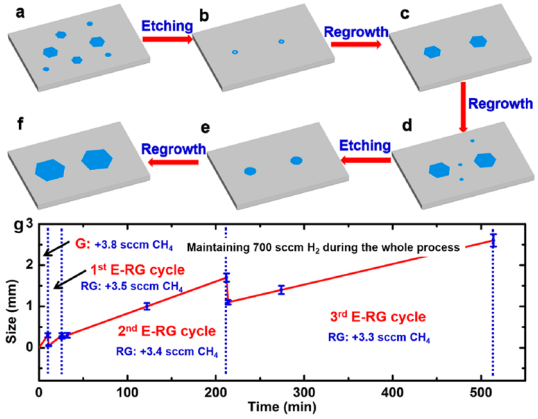

Figure 1. Scheme depicting the G−rE−RG process. (a) CVD growth of graphene domains on a substrate. (b) Hydrogen etching to reduce domain density. (c) Regrowth of the etched graphene domains. (d) New nuclei appear on the substrate during regrowth. (e) Hydrogen etching to remove the new nuclei generated during regrowth. (f) Large-size single-crystal graphene domains obtained by the G−rE−RG method. (g) Schematic of the G−rE−RG process used for fabricating ~3 mm single-crystal graphene domains, with the flow rates of CH_4 and H_2 used. The reaction temperature was 1060 °C during the whole process. The error bars show the size range of the single-crystal graphene domains obtained under the same conditions, and the blue dots in the middle of the error bars represent the average size of graphene domains.

RESULTS AND DISCUSSION

The G−rE−RG process is illustrated in Figure 1. First, we grew single-crystal graphene domains on a Pt substrate with normal CVD growth conditions (Figure 1a). As reported previously,[31] not all the graphene domains nucleated at the same time and therefore had different sizes after a certain growth time. This size difference means that some domains are etched away while some remain after etching given that the etching rate is almost the same for all domains. We therefore then changed from a growth condition to an etching condition to induce graphene etching (Figure 1b). With increasing etching time, the graphene domains continuously shrank. After a certain time, most graphene domains were etched away, and only a few small domains remained, corresponding to the initial large domains formed during CVD growth. Theoretically, we can obtain a very low nucleation density, even one nucleus on a wafer, by making the etching time long enough. After etching, we regrew the etched graphene domains by returning to a growth condition (Figure 1c). As soon as new graphene nuclei appeared on the uncovered region of the substrate (Figure 1d), we carried out a second E−RG cycle (Figure 1e and f). After several E−RG cycles, large-area single-crystal graphene domains were obtained. Theoretically, wafer-size single-crystal graphene can be fabricated if the growth time is not important and the facility can be run for a very long time at high temperature.

We have investigated graphene growth behavior as a function of methane flow rate for conventional CVD

and found that, with decreasing methane flow rate, the nucleation density of graphene was greatly decreased, but the growth rate was also dramatically decreased and a remarkably long incubation time was necessary for graphene nucleation (Figure S1 and Table S2). We suggest that the incubation period is a process to accumulate carbon species in a Pt substrate with the decomposition of method to achieve a critical supersaturation level to overcome the energy barrier for graphene nucleation.[32] The above facts mean that it is impossible to simultaneously realize a low nucleation density and high growth rate by conventional CVD. For instance, the nucleation density was ~300/cm^2, 3/cm^2, and 1/cm^2 for methane flow rates of 3.7, 3.4, and 3.3 sccm, respectively. A ~300 μm graphene domain can be fabricated in 20 min using a methane flow rate of 3.7 sccm, but in sharp contrast, no visible nuclei were observed by scanning electron microscope (SEM) after 4 and 7 h growth for methane flow rates of 3.4 and 3.3 sccm. The mean growth rate of graphene was roughly estimated to be ~900, 18, and 2 μm/h for methane flow rates of 3.7, 3.4, and 3.3 sccm, respectively, when considering the incubation time. Therefore, it is unrealistic to use a very low methane flow rate to fabricate large-area single-crystal graphene because of the very low growth rate and remarkably long incubation time even though the nucleation density is very low, not to mention the inevitable random nucleation during graphene growth.

To fabricate large-area single-crystal graphene with a high growth rate, we changed the methane flow rate during the whole G−rE−RG process so that it decreased with the number of growth cycles. Figure 1g and Figure 2 show the experimental process and conditions used for fabricating ~3 mm single-crystal graphene domains by the G−rE−RG method and the typical single-crystal graphene domains obtained at different stages in the process. A high methane flow rate in the initial growth enables rapid nucleation and growth of graphene domains. After 10 min growth, ~250 μm size hexagonal single-crystal graphene domains were obtained (Figure 2a). Then we switched off the methane and used pure hydrogen to induce etching. After 1 min hydrogen etching, most small domains were etched away and only a very few domains survived, dramatically reducing the domain density. Note that there is only one single domain left in a region of ~3 × 3 mm^2 (Figure 2b and Figure S2). As mentioned above, a long incubation time is required for graphene nucleation at a low methane flow rate. Therefore, after each etching, we used a lower methane flow rate than in the previous growth cycle to induce regrowth, which ensures that the surviving graphene domain has a longer growth time before new nuclei appear. It is important to note that the very long incubation time for a low methane flow rate is avoided in this G−rE−RG process, which is helpful to realize a high average growth rate over the whole fabrication process. The domain became larger than that obtained in the previous cycle when new nuclei appeared and grew to ~100 μm (Figure 2c and e). We then carried out further etching using pure hydrogen. This ensured only one domain remained in a region of ~3 × 3 mm^2 even though it became larger (Figure 2g and h). It is needed to point out that the single-crystal graphene domains actually experienced a series of edge structure and shape evolution during etching and regrowth processes, as shown in ref 31.

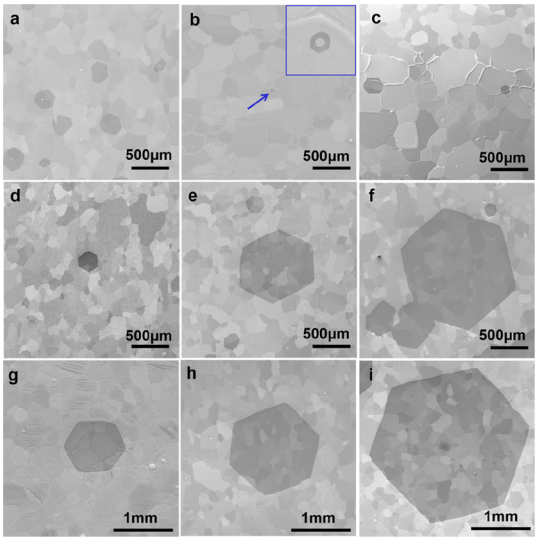

Figure 2. SEM images of single-crystal graphene domains at different stages during the G−rE−RG process. (a) Initial growth stage for 10 min. (b) Domains from (a) after 1 min etching in the first E−RG cycle. The inset shows the high-magnification SEM image of the graphene domain indicated by a blue arrow. (c) Domains from (b) after 15 min regrowth in the first E−RG cycle. (d−f) Domains after (d) 5 min, (e) 1.5 h, and (f) 3 h regrowth in the second E−RG cycle. (g−i) Domains after (g) 2 min etching from (f) and then for (h) 1 h and (i) 5 h regrowth from (g) in the third E−RG cycle.

After three cycles of E-RG, we obtained single-crystal graphene domains of ~3 mm in average size (Figure 2i). This G−rE−RG method is unique in the following respects: (1) we can grow ~3 mm single-crystal graphene domains with an initial nucleation density of only ~2/mm^2 when it is impossible to grow domains larger than 1 mm by conventional CVD; (2) the ~3 mm single-crystal graphene domains grew with a high average growth rate of ~7 μm/min, which is impossible to achieve by conventional CVD, in which the growth rate is ~2 μm/h (*i.e.*, ~0.03 μm/min). In addition, it is worth noting that there are nearly no additional layers observed in the single-crystal graphene domains fabricated by our G−rE−RG method (Figure 2c−f, h, and i). In contrast, many small additional layers are usually formed during the growth of single-crystal graphene domains by conventional CVD especially the two-step CVD method.[20−22,24,27,28] It is well known that the edges of graphene have much higher chemical reactivity than its interior

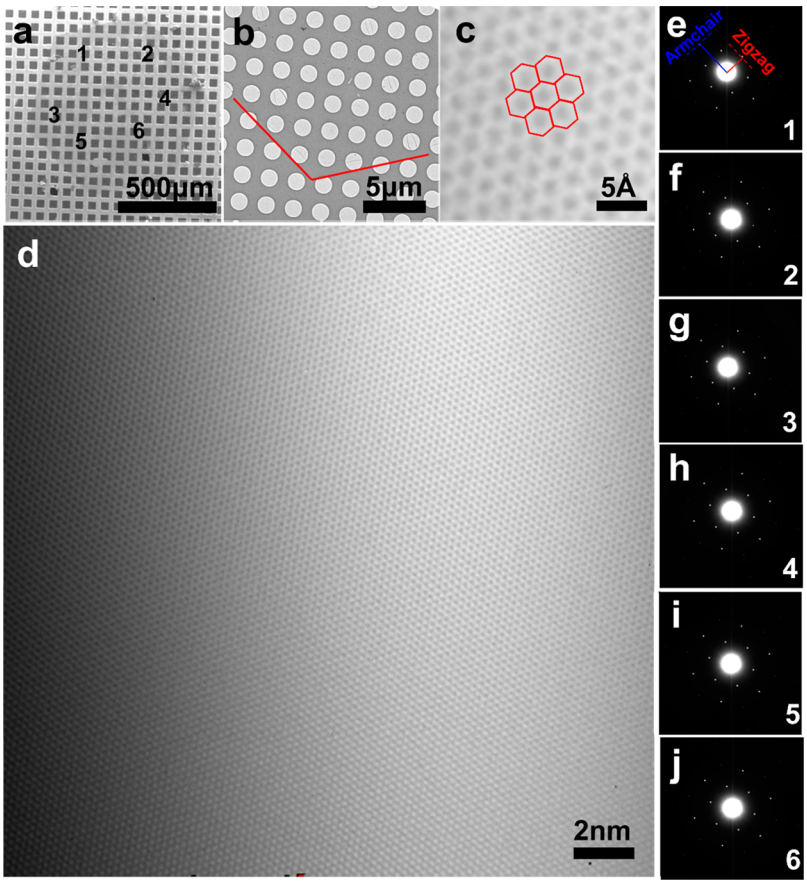

Figure 3. Structural characterization of a single-crystal graphene domain produced by G−rE−RG. (a) SEM image of a ~1 mm sized hexagonal domain transferred to a TEM grid by the electrochemical bubbling method.[20] (b) Low-magnification TEM image of the edge region of the domain in (a). The red lines indicate graphene edges. (c, d) Aberration-corrected and monochromated TEM images of the domain, showing a perfect carbon lattice with 6-fold symmetry without any structural defects or disorder. (e−j) SAED patterns taken from the six areas in (a) labeled 1−6. Red and blue dotted lines respectively indicate the zigzag and armchair directions determined by SAED.

region; therefore, the small graphene additional layers formed in the CVD growth process are preferentially etched away during the following etching process. Note that the additional layers are usually formed at the defect sites in graphene domains such as the nucleation sites.[20−22,24,27,28] Therefore, we suggest that the lack of additional layers in the single-crystal graphene domains by G−rE−RG is attributed to their defect-free nature, as discussed below.

Another very important feature of the G−rE−RG method is the efficient healing of the structural defects that are generated during the initial CVD growth. A core−shell structured C_{21}, which is composed of three isolated pentagons and four hexagons, has been predicted as an initial stable cluster on a metal surface for the nucleation of graphene.[33] In addition to these nucleation defects, it has been observed experimentally that there are many kinds of defects in CVD-grown or even mechanically exfoliated graphene such as topological defects, single vacancies, multiple vacancies, carbon adatoms, and dislocations.[12,34−38] Theoretically, the energy barriers to the formation of all these defects are significantly reduced in the presence of a metal surface compared to those in suspended graphene.[39] More importantly, CVD is a nonequilibrium process during which the attachment of carbon atoms to the edges of graphene can be easily disturbed by experimental conditions such as small fluctuations in reaction temperature and gas atmosphere, as well as defects and impurities in the substrates and the substrate roughness. Therefore, the formation of defects is inevitable in CVD-grown graphene. Actually, many hexagonal holes appeared in single-crystal graphene domains grown by conventional CVD after etching (Figure S3). Taking into account the preferential etching of defects due to their high formation energy, this fact confirms the presence of defects in the single-crystal graphene fabricated by conventional CVD.

However, it is important to note that no visible holes appeared in the single-crystal graphene domains grown by this G−rE−RG (Figure 2g), consistent with our previous observations on the regrown graphene from an etched domain,[31] indicating that the defects have been effectively healed. Theoretically, the healing of defects by high-temperature CVD is reasonable.

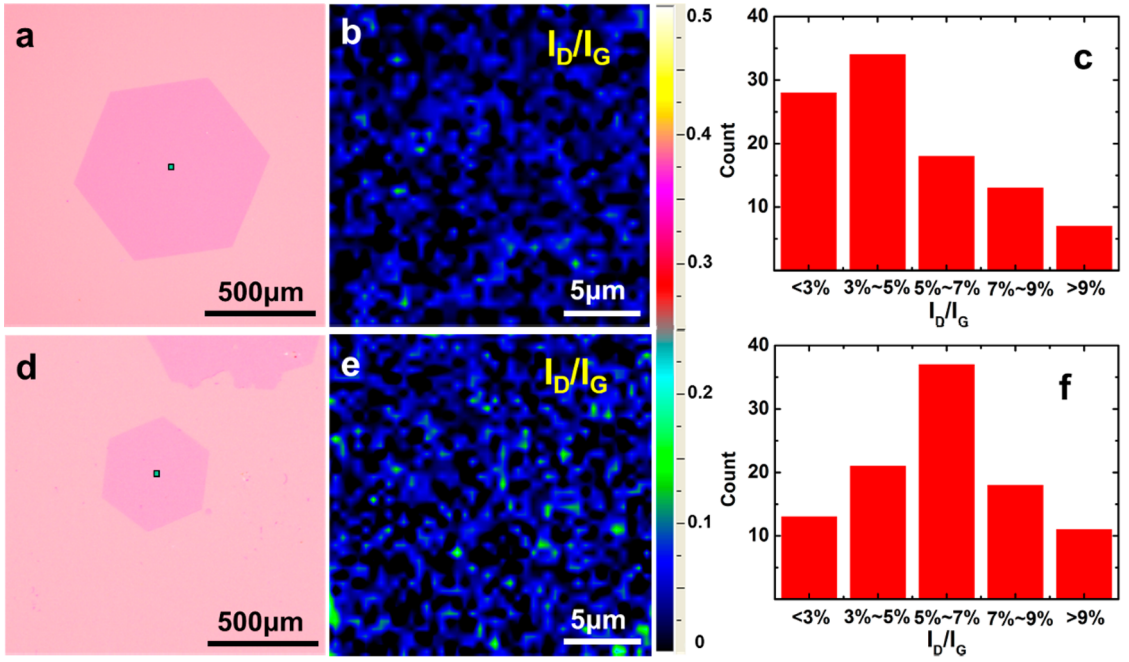

Figure 4. Optical and Raman characterization of single-crystal graphene domains grown by (a,b,c) G−rE−RG and (d,e,f) conventional CVD (a, d) Optical images; (b, e) I_D/I_G Raman mappings of the regions indicated by the squares in (a, d) and (c, f) histograms of I_D/I_G values over the whole area of the domains in (a,d).

First, the transformation of defects to a perfect hexagonal carbon lattice is energetically favorable because of the higher formation energy of defects.[40,41] Second, the perfect hexagonal shape of the holes formed from defects during etching indicates that these holes can be filled up by only hexagonal carbon clusters (Figure 2b, Figure S3 and ref 31). Experimentally, the use of a very low methane flow rate in the later growth cycles is essential since it facilitates the relaxation of a carbon−metal system toward the thermal equilibrium state to heal defects. This assertion is proved by the fact that, after etching, more holes appeared in domains grown at a high methane flow rate than in those grown at a low flow rate (Figure S3).

In order to heal defects in carbon materials such as graphite,[42] carbon nanotubes,[43] and reduced graphene oxide,[44] long-time high-temperature annealing at more than 2000 °C in an inert atmosphere (graphitization) is required.[42−44] In contrast, our G−rE−RG method can heal the defects very rapidly (~7 μm/min) at a much lower temperature (~1000 °C). During graphitization, carbon atoms need to overcome a series of high-energy barriers of usually more than 5 eV for rotation, rupture, and re-forming of carbon−carbon bonds to remove defects and form a perfect hexagonal carbon lattice.[41] However, healing defects by the E−RG process requires only the rupture and re-forming of carbon−carbon bonds, which requires an energy barrier of only ~2−3 eV to be overcome.[45] Moreover, the presence of the metal substrate can greatly reduce these energy barriers.[45] Therefore, healing defects by our G−rE−RG method requires less energy and can be realized much easier than high-temperature graphitization, which is impossible to realize for conventional CVD.

We used transmission electron microscopy (TEM) to characterize the detailed structure of graphene domains produced by G−rE−RG (Figure 3). With an aberration-corrected and monochromated TEM, we are able to image the atomic structure of a suspended single-crystal graphene domain. A low electron beam voltage of 60 kV minimized electron beam irradiation damage to the graphene.[46] As shown in Figure 3c and d, the 6-fold symmetry of the graphene lattice was well observed without any vacancies, topological defects, and carbon adatoms and dislocations. Importantly, extensive measurements on this graphene domain and many other domains gave a similar result. We performed selected-area electron diffraction (SAED) measurements on 30 areas in a graphene domain. All areas showed the same electron diffraction patterns as those shown in Figure 3e−j, unambiguously confirming the single-crystalline nature of the graphene domain across its entire area. Moreover, the angles between the zigzag direction determined by SAED and the edge direction in real space is 0 degree, suggesting the edges of the single-crystal graphene have a zigzag orientation.[7] which is consistent with the results previously reported for single-crystal graphene domains grown by conventional CVD (Table S1 and refs 17, 20, 22, 24).

Raman spectroscopy is a powerful tool to characterize the number of layers, defects, strain, and the effects of perturbations of graphene over a much larger area than aberration-corrected and monochromated

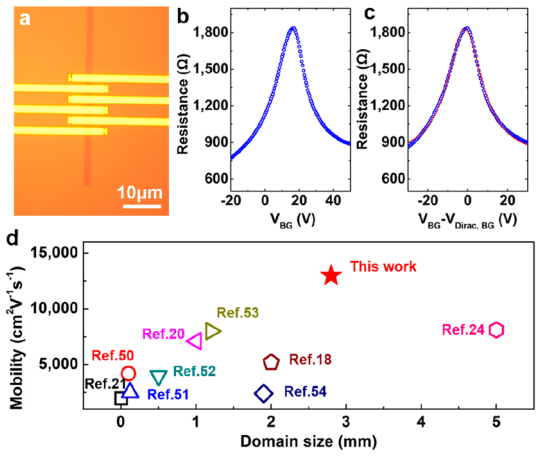

Figure 5. Transport properties of the single-crystal graphene domains fabricated by G−rE−RG. (a) Optical microscopy image of a back-gate graphene FET on a SiO_2/Si substrate. (b) Device resistance *versus* back-gate voltage (V_{BG}) of this graphene FET. (c) Device resistance *versus* $V_{BG} - V_{Dirac,BG}$ (VBG at the Dirac point) and a fitted curve (solid red line). (d) Electron mobility comparison of the single-crystal graphene domains produced by our G−rE−RG method (indicated by a red star) and those produced by conventional CVD reported in the literature.[18,20,21,24,50−54] All the data were measured with FET devices under ambient conditions.

TEM.[47,48] We measured a number of Raman spectra and mappings of the graphene domains fabricated by our G−rE−RG method and conventional CVD. We used the peak area ratio of D band to G band (I_D/I_G) to evaluate defects in the samples because the D band is almost invisible (Figure S4 and ref 49). Note that the single-crystal graphene domain produced by G−rE−RG shows a smaller area of visible I_D/I_G (Figure 4b) than does one produced by conventional CVD (Figure 4e). Moreover, most of the I_D/I_G data for the former sample are in the range 3−5% (Figure 4c), which is much lower than values measured on the latter sample (5−7%, Figure 4f). All these results confirm that the single-crystal graphene domains fabricated by G−rE−RG have fewer defects than those produced by conventional CVD.

To evaluate the electronic quality of our single-crystal graphene domains, we fabricated back-gate field-effect transistors (FETs) on Si/SiO_2 substrates, using Ti/Au (5/45 nm) as source and drain electrodes (Figure 5a). All the transport characteristics of the devices were measured under ambient conditions. We then used a device model that combines the minimum carrier density at the Dirac point and the dielectric and quantum capacitances to fit the measured data to extract carrier mobility. Figure 5b and c show typical measured and fitted data, respectively. The extracted carrier mobility for this device was ~13 000 $cm^2\ V^{-1}\ s^{-1}$ with a residual carrier density at the Dirac point of ~4.1 × 10^{11} cm^{-2}. Under similar measurement conditions, this value is about double the mobility (~7000 $cm^2\ V^{-1}\ s^{-1}$) of a single-crystal graphene domain produced by conventional CVD on Pt[20] and much larger than those (up to ~8000 $cm^2\ V^{-1}\ s^{-1}$) of domains produced by conventional CVD on Cu that have been reported so far (Figure 5d and Table S1).[18,21,24,50−54] Such a high mobility further confirms the defect-free nature of our graphene domains, consistent with HRTEM observations and Raman measurements.

CONCLUSIONS

In conclusion, we have developed a G−rE−RG method to fabricate large-area defect-free single-crystal graphene domains, where the methane flow rate is decreased with the number of growth cycles. Through etching, we are able to efficiently remove randomly nucleated domains and reveal structural defects generated during CVD growth. Regrowth not only provides carbon atoms to the graphene edges to induce its further growth but also plays a role in healing the structural defects at a much faster rate. Using this method, we obtained ~3 mm single-crystal graphene domains on a Pt substrate, which show a carrier mobility up to 13 000 $cm^2\ V^{-1}\ s^{-1}$ under ambient conditions. Combining this G−rE−RG method with other strategies to reduce the nucleation density of graphene such as polishing the substrate and introducing oxygen into reaction systems, it is expected that much larger, even wafer size, defect-free single-crystal graphene may be produced.

EXPERIMENTAL SECTION

G−rE−RG CVD Growth of Large-Area Defect-Free Single-Crystal Graphene. A piece of Pt foil (180 μm thick, 99.9 wt % metal basis, 10 mm × 20 mm) was first rinsed with acetone and ethanol for 1 h each and then loaded into a fused silica reaction tube (inner diameter: 22 mm), heated to 1060 °C under the protection of H_2 (700 sccm), and annealed for 10 min to remove residual carbon or organic substances. Growth was then started by introducing methane and maintained for a certain time. After CVD growth, the methane flow was cut off while the other parameters were held constant to induce graphene etching. After etching for a certain time, methane was reintroduced for graphene regrowth. To grow ~3 mm single-crystal graphene domains, three cycles of etching−regrowth were used. Detailed experimental conditions are given in Figure 1g. When the reaction was over, the Pt foil was quickly pulled out of the high-temperature zone, the furnace shut down, and the methane flow was turned off when the furnace temperature was lower than 800 °C.

Characterization. The Pt foil covered by graphene domains was taken out for size and morphological analysis by SEM (Nova NanoSEM 430, acceleration voltage of 5 kV). Using the electrochemical bubbling transfer method,[20] the graphene domains were transferred onto a Si/SiO_2 (290 nm) substrate or a TEM grid. Optical microscopy (Nikon LV100D), Raman spectroscopy (JY HR800, 532 nm laser wavelength, 1 μm spot size, 1 s integration time, laser power below 2 mW), and TEM (FEI Tecnai T12, 120 kV; Titan^3 G2 60-300 S/TEM, 60 kV) were used to identify the quality and structure of the graphene domains. Aberration-corrected and monochromated TEM was used at 60 kV in a

high-vacuum environment to minimize electron-beam-induced damage to the suspended single-crystal graphene domains.[46]

Conflict of Interest: The authors declare no competing financial interest.

Acknowledgment. The authors thank Dr. Lichang Yin for valuable discussions. This work was supported by the National Science Foundation of China (Nos. 51325205, 51290273, 51221264, 51172240, and 51102241), the Ministry of Science and Technology of China (No. 2012AA030303), and the Chinese Academy of Sciences (No. KGZD-EW-303-1).

Supporting Information Available: Figures S1–S4, Tables S1 and S2, and references 55–59. This material is available free of charge *via* the Internet at http://pubs.acs.org

REFERENCES AND NOTES

1. Novoselov, K. S.; Geim, A. K.; Morozov, S. V.; Jiang, D.; Zhang, Y.; Dubonos, S. V.; Grigorieva, I. V.; Firsov, A. A. Electric Field Effect in Atomically Thin Carbon Films. *Science* **2004**, *306*, 666–669.
2. Geim, A. K. Graphene: Status and Prospects. *Science* **2009**, *324*, 1530–1534.
3. Geim, A. K.; Novoselov, K. S. The Rise of Graphene. *Nat. Mater.* **2007**, *6*, 183–191.
4. Wei, D.; Liu, Y. Controllable Synthesis of Graphene and Its Applications. *Adv. Mater.* **2010**, *22*, 3225–3241.
5. Huang, P. Y.; Ruiz-Vargas, C. S.; van der Zande, A. M.; Whitney, W. S.; Levendorf, M. P.; Kevek, J. W.; Garg, S.; Alden, J. S.; Hustedt, C. J.; Zhu, Y.; et al. Grains and Grain Bound`aries in Single-Layer Graphene Atomic Patchwork Quilts. *Nature* **2011**, *469*, 389–392.
6. Yazyev, O. V.; Louie, S. G. Electronic Transport in Polycrystalline Graphene. *Nat. Mater.* **2010**, *9*, 806–809.
7. Yu, Q.; Jauregui, L. A.; Wu, W.; Colby, R.; Tian, J.; Su, Z.; Cao, H.; Liu, Z.; Pandey, D.; Wei, D.; et al. Control and Characterization of Individual Grains and Grain Boundaries in Graphene Grown by Chemical Vapour Deposition. *Nat. Mater.* **2011**, *10*, 443–449.
8. Rasool, H. I.; Ophus, C.; Klug, W. S.; Zettl, A.; Gimzewski, J. K. Measurement of the Intrinsic Strength of Crystalline and Polycrystalline Graphene. *Nat. Commun.* **2013**, *4*, 2811.
9. Wei, Y.; Wu, J.; Yin, H.; Shi, X.; Yang, R.; Dresselhaus, M. The Nature of Strength Enhancement and Weakening by Pentagon–Heptagon Defects In graphene. *Nat. Mater.* **2012**, *11*, 759–763.
10. Grantab, R.; Shenoy, V. B.; Ruoff, R. S. Anomalous Strength Characteristics of Tilt Grain Boundaries in Graphene. *Science* **2010**, *330*, 946–948.
11. Lee, G. H.; Cooper, R. C.; An, S. J.; Lee, S.; van der Zande, A.; Petrone, N.; Hammerberg, A. G.; Lee, C.; Crawford, B.; Oliver, W.; et al. High-Strength Chemical-Vapor-Deposited Graphene and Grain Boundaries. *Science* **2013**, *340*, 1073–1076.
12. Banhart, F.; Kotakoski, J.; Krasheninnikov, A. V. Structural Defects in Graphene. *ACS Nano* **2011**, *5*, 26–41.
13. Lahiri, J.; Lin, Y.; Bozkurt, P.; Oleynik, I. I.; Batzill, M. An Extended Defect in Graphene as a Metallic Wire. *Nat. Nanotechnol.* **2010**, *5*, 326–329.
14. Oleg, V. Y. Emergence of Magnetism in Graphene Materials and Nanostructures. *Rep. Prog. Phys.* **2010**, *73*, 056501.
15. Rutter, G. M.; Crain, J. N.; Guisinger, N. P.; Li, T.; First, P. N.; Stroscio, J. A. Scattering and Interference in Epitaxial Graphene. *Science* **2007**, *317*, 219–222.
16. Ugeda, M. M.; Brihuega, I.; Guinea, F.; Gomez-Rodriguez, J. M. Missing Atom as a Source of Carbon Magnetism. *Phys. Rev. Lett.* **2010**, *104*, 096804.
17. Yan, Z.; Lin, J.; Peng, Z.; Sun, Z.; Zhu, Y.; Li, L.; Xiang, C.; Samuel, E. L.; Kittrell, C.; Tour, J. M. Toward the Synthesis of Wafer-Scale Single-Crystal Graphene on Copper Foils. *ACS Nano* **2012**, *6*, 9110–9117.
18. Chen, S.; Ji, H.; Chou, H.; Li, Q.; Li, H.; Suk, J. W.; Piner, R.; Liao, L.; Cai, W.; Ruoff, R. S. Millimeter-Size Single-Crystal Graphene by Suppressing Evaporative Loss of Cu During Low Pressure Chemical Vapor Deposition. *Adv. Mater.* **2013**, *25*, 2062–2065.
19. Wang, H.; Wang, G.; Bao, P.; Yang, S.; Zhu, W.; Xie, X.; Zhang, W. J. Controllable Synthesis of Submillimeter Single-Crystal Monolayer Graphene Domains on Copper Foils by Suppressing Nucleation. *J. Am. Chem. Soc.* **2012**, *134*, 3627–3630.
20. Gao, L.; Ren, W.; Xu, H.; Jin, L.; Wang, Z.; Ma, T.; Ma, L. P.; Zhang, Z.; Fu, Q.; Peng, L. M.; et al. Repeated Growth and Bubbling Transfer of Graphene with Millimetre-Size Single-Crystal Grains Using Platinum. *Nat. Commun.* **2012**, *3*, 699.
21. Wu, B.; Geng, D.; Guo, Y.; Huang, L.; Xue, Y.; Zheng, J.; Chen, J.; Yu, G.; Liu, Y.; Jiang, L.; et al. Equiangular Hexagon-Shape-Controlled Synthesis of Graphene on Copper Surface. *Adv. Mater.* **2011**, *23*, 3522–3525.
22. Vlassiouk, I.; Regmi, M.; Fulvio, P.; Dai, S.; Datskos, P.; Eres, G.; Smirnov, S. Role of Hydrogen in Chemical Vapor Deposition Growth of Large Single-Crystal Graphene. *ACS Nano* **2011**, *5*, 6069–6076.
23. Hao, Y.; Bharathi, M. S.; Wang, L.; Liu, Y.; Chen, H.; Nie, S.; Wang, X.; Chou, H.; Tan, C.; Fallahazad, B.; et al. The Role of Surface Oxygen in the Growth of Large Single-Crystal Graphene on Copper. *Science* **2013**, *342*, 720–723.
24. Zhou, H.; Yu, W. J.; Liu, L.; Cheng, R.; Chen, Y.; Huang, X.; Liu, Y.; Wang, Y.; Huang, Y.; Duan, X. Chemical Vapour Deposition Growth of Large Single Crystals of Monolayer and Bilayer Graphene. *Nat. Commun.* **2013**, *4*, 2096.
25. Gan, L.; Luo, Z. Turning Off Hydrogen to Realize Seeded Growth of Subcentimeter Single-Crystal Graphene Grains on Copper. *ACS Nano* **2013**, *7*, 9480–9488.
26. Lee, J. H.; Lee, E. K.; Joo, W. J.; Jang, Y.; Kim, B. S.; Lim, J. Y.; Choi, S. H.; Ahn, S. J.; Ahn, J. R.; Park, M. H.; et al. Wafer-Scale Growth of Single-Crystal Monolayer Graphene on Reusable Hydrogen-Terminated Germanium. *Science* **2014**, *344*, 286–289.
27. Gan, L.; Ou, X. W.; Zhang, Q. C.; Wu, R. Z.; Luo, Z. T. Graphene Amplification by Continued Growth on Seed Edges. *Chem. Mater.* **2014**, *26*, 4137–4143.
28. Wang, H.; Wang, G. Z.; Bao, P. F.; Shao, Z. B.; Zhang, X.; Yang, S. L.; Zhu, W.; Deng, B. C. Lateral Homoepitaxial Growth of Graphene. *CrystEngComm* **2014**, *16*, 2593–2597.
29. Bolotin, K. I.; Sikes, K. J.; Jiang, Z.; Klima, M.; Fudenberg, G.; Hone, J.; Kim, P.; Stormer, H. L. Ultrahigh Electron Mobility in Suspended Graphene. *Solid State Commun.* **2008**, *146*, 351–355.
30. Hwang, E. H.; Adam, S.; Sarma, S. D. Carrier Transport in Two-Dimensional Graphene Layers. *Phys. Rev. Lett.* **2007**, *98*, 186806.
31. Ma, T.; Ren, W.; Zhang, X.; Liu, Z.; Gao, Y.; Yin, L. C.; Ma, X. L.; Ding, F.; Cheng, H. M. Edge-Controlled Growth and Kinetics of Single-Crystal Graphene Domains by Chemical Vapor Deposition. *Proc. Natl. Acad. Sci. U. S. A.* **2013**, *110*, 20386–20391.
32. Kim, H.; Mattevi, C.; Calvo, M. R.; Oberg, J. C.; Artiglia, L.; Agnoli, S.; Hirjibehedin, C. F.; Chhowalla, M.; Saiz, E. Activation Energy Paths for Graphene Nucleation and Growth on Cu. *ACS Nano* **2012**, *6*, 3614–3623.
33. Yuan, Q.; Gao, J.; Shu, H.; Zhao, J.; Chen, X.; Ding, F. Magic Carbon Clusters in the Chemical Vapor Deposition Growth of Graphene. *J. Am. Chem. Soc.* **2012**, *134*, 2970–2975.
34. Alden, J. S.; Tsen, A. W.; Huang, P. Y.; Hovden, R.; Brown, L.; Park, J.; Muller, D. A.; McEuen, P. L. Strain Solitons and Topological Defects in Bilayer Graphene. *Proc. Natl. Acad. Sci. U. S. A.* **2013**, *110*, 11256–11260.
35. Meyer, J. C.; Kisielowski, C.; Erni, R.; Rossell, M. D.; Crommie, M. F.; Zettl, A. Direct Imaging of Lattice Atoms and Topological Defects in Graphene Membranes. *Nano Lett.* **2008**, *8*, 3582–3586.
36. Robertson, A. W.; Warner, J. H. Atomic Resolution Imaging of Graphene by Transmission Electron Microscopy. *Nanoscale* **2013**, *5*, 4079–4093.
37. Robertson, A. W.; Montanari, B.; He, K.; Allen, C. S.; Wu, Y. A.; Harrison, N. M.; Kirkland, A. I.; Warner, J. H. Structural Reconstruction of the Graphene Monovacancy. *ACS Nano* **2013**, *7*, 4495–4502.

38. Robertson, A. W.; Lee, G. D.; He, K.; Yoon, E.; Kirkland, A. I.; Warner, J. H. Stability and Dynamics of the Tetravacancy in Graphene. *Nano Lett.* **2014**, *14*, 1634–1642.
39. Wang, L.; Zhang, X.; Chan, H. L.; Yan, F.; Ding, F. Formation and Healing of Vacancies in Graphene Chemical Vapor Deposition (CVD) Growth. *J. Am. Chem. Soc.* **2013**, *135*, 4476–4482.
40. Li, L.; Reich, S.; Robertson, J. Defect Energies of Graphite: Density-Functional Calculations. *Phys. Rev. B* **2005**, *72*, 184109.
41. Ma, J.; Alfè, D.; Michaelides, A.; Wang, E. Stone-Wales Defects in Graphene and Other Planar sp^2-bonded materials. *Phys. Rev. B* **2009**, *80*, 033407.
42. Goma, J.; Oberlin, M. Graphitization of Thin Carbon-Films. *Thin Solid Films* **1980**, *65*, 221–232.
43. Andrews, R.; Jacques, D.; Qian, D.; Dickey, E. C. Purification and Structural Annealing of Multiwalled Carbon Nanotubes at Graphitization Temperatures. *Carbon* **2001**, *39*, 1681–1687.
44. Rozada, R.; Paredes, J. I.; Villar-Rodil, S.; Martinez-Alonso, A.; Tascon, J. M. D. Towards Full Repair of Defects in Reduced Graphene Oxide Films by Two-Step Graphitization. *Nano Res.* **2013**, *6*, 216–233.
45. Maier, K.; Peo, M.; Saile, B.; Schaefer, H. E.; Seeger, A. High−Temperature Positron Annihilation and Vacancy Formation in Refractory Metals. *Philos. Mag. A* **1979**, *40*, 701–728.
46. Meyer, J. C.; Eder, F.; Kurasch, S.; Skakalova, V.; Kotakoski, J.; Park, H. J.; Roth, S.; Chuvilin, A.; Eyhusen, S.; Benner, G.; et al. Accurate Measurement of Electron Beam Induced Displacement Cross Sections for Single-Layer Graphene. *Phys. Rev. Lett.* **2012**, *108*, 196102.
47. Ferrari, A. C.; Meyer, J. C.; Scardaci, V.; Casiraghi, C.; Lazzeri, M.; Mauri, F.; Piscanec, S.; Jiang, D.; Novoselov, K. S.; Roth, S.; et al. Raman Spectrum of Graphene and Graphene Layers. *Phys. Rev. Lett.* **2006**, *97*, 187401.
48. Ferrari, A. C.; Basko, D. M. Raman Spectroscopy as a Versatile Tool for Studying the Properties of Graphene. *Nat. Nanotechnol.* **2013**, *8*, 235–246.
49. Martins Ferreira, E. H.; Moutinho, M. V. O.; Stavale, F.; Lucchese, M. M.; Capaz, R. B.; Achete, C. A.; Jorio, A. Evolution of the Raman Spectra from Single-, Few-, and Many-Layer Graphene with Increasing Disorder. *Phys. Rev. B* **2010**, *82*, 125429.
50. Zhang, Y.; Zhang, L.; Kim, P.; Ge, M.; Li, Z.; Zhou, C. Vapor Trapping Growth of Single-Crystalline Graphene Flowers: Synthesis, Morphology, and Electronic Properties. *Nano Lett.* **2012**, *12*, 2810–2816.
51. Geng, D.; Wu, B.; Guo, Y.; Huang, L.; Xue, Y.; Chen, J.; Yu, G.; Jiang, L.; Hu, W.; Liu, Y. Uniform Hexagonal Graphene Flakes and Films Grown on Liquid Copper Surface. *Proc. Natl. Acad. Sci. U. S. A.* **2012**, *109*, 7992–7996.
52. Li, X.; Magnuson, C. W.; Venugopal, A.; Tromp, R. M.; Hannon, J. B.; Vogel, E. M.; Colombo, L.; Ruoff, R. S. Large-Area Graphene Single Crystals Grown by Low-Pressure Chemical Vapor Deposition of Methane on Copper. *J. Am. Chem. Soc.* **2011**, *133*, 2816–2819.
53. Wu, T. R.; Ding, G. Q.; Shen, H. L.; Wang, H. M.; Sun, L.; Jiang, D.; Xie, X. M.; Jiang, M. H. Triggering the Continuous Growth of Graphene toward Millimeter-Sized Grains. *Adv. Funct. Mater.* **2013**, *23*, 198–203.
54. Wang, C.; Chen, W.; Han, C.; Wang, G.; Tang, B.; Tang, C.; Wang, Y.; Zou, W.; Chen, W.; Zhang, X. A.; et al. Growth of Millimeter-Size Single Crystal Graphene on Cu Foils by Circumfluence Chemical Vapor Deposition. *Sci. Rep.* **2014**, *4*, 4537.